Open Access

Article Type: Research Article

Volume 1 Issue 1 - 2023

SCIBASE Journals

SciBase Oncology

Cytotoxicity and Genotoxicity Effects of Intravenous Injection of 50 nm Gold Nanorods (AuNRs) in Dogs

Ahmed Sabry S Abdoon[1]*; Omaima M Kandil[1]; Emad A Al Ashkar[2]; Badawi A Anis[2]; Amina A Gamal ElDin[3]; Ashraf H Shaalan[4]

[1]Department of Animal Reproduction, Veterinary Research Institute, National Research Center (NRC, Egypt), Egypt.

[2]Spectroscopy Department, Physics Institute, NRC, Egypt.

[3]Pathology Department, Medical Research Institute, NRC, Egypt.

[4]Biological Anthropology Department, Medical Research Institute, NRC, Egypt.

Corresponding Author: Ahmed Sabry S Abdoon

Department of Animal Reproduction and Artificial Insemination, Veterinary Research Institute, National Research Centre (NRC), Tahrir St., Dokki 12622, Cairo, Egypt.

Tel: +20 1001662430 & +20 233370931;

Email: assabdoon@yahoo.com

Article information

Received: Aug 17, 2023

Accepted: Oct 09, 2023

Published: Oct 16, 2023

SciBase Oncology - scibasejournals.org

Citation: Ahmed Sabry SA, Omaima MK, Emad AAA, Badawi AA, Gamal ElDin AA. Cytotoxicity and Genotoxicity Effects of Intravenous Injection of 50 nm Gold Nanorods (AuNRs) in Dogs. SciBase Oncol. 2023; 1(1): 1004.

Abstract

This work was designed to investigate the possible acute and long-term acute toxicity of intravenous (i.v.) injection of 50 nm gold nanorods (AuNRs) in dogs. Eighteen native dogs were divided into control (n=8); acute toxicity (n=5), and long-term acute toxicity (n=5). Dogs were i.v. injected with 75 µg of 50 nm AuNRs/kg vs. saline solution in the control group. In the acute toxicity, blood samples were collected from control and AuNRs groups on days 3 and 14 after the AuNRs injection. In long-term toxicity, blood samples from control and AuNRs injected animals were collected monthly (up to 6 months). Blood was used for CBC, liver, and kidney functions, cell viability, and genotoxicity. Hepatic, splenic, and renal tissue biopsies were obtained on day 14 (acute toxicity) or after the 6th month in the long-term acute toxicity study for histopathology, Caspase-3 protein expression using immunohistochemistry, Results showed no aberrant clinical signs, or gross morphological changes in liver, kidney, and spleen were detected after AuNRs injection. AuNRs produced mild histopathological changes in the hepatic and renal tissues in the long-term acute toxicity group. 50 nm AuNRs produced mild and reversible changes in blood, liver, and kidney parameters. 50 nm AuNRs significantly increase the expression of Caspase-3 protein expression, decrease the cell viability, and increase % DNA fragmentation of PWBCs.

Conclusion: i.v. injection of 50 nm AuNRs could induce blood hemolysis, and affect blood profile, liver and kidney functions, decrease the cell viability of PWBCs through the Caspase-3 pathway, and genotoxicity.

Keywords: Dogs; AuNRs; Toxicity; Blood profile and biochemistry; Histopathology; TEM; Genotoxicity.

Introduction

Currently, cancer is representing a great health challenge worldwide [1]. Many strategies such as surgery, checkpoint inhibitors, chemotherapy, immunotherapy, and radiation therapy have been used for the treatment of cancer [2]. However, these approaches not only target cancer cells but also affect normal tissues yielding poor therapeutic outcomes. Nanomedicine, the medical applications of nanomaterials and nanodevices, is currently used to solve these problems. In nanomedicine, gold nanoparticles (AuNPs) are promising agents for diagnosis, drug/gene delivery, imaging, and targeted Photothermal Therapy (PTT) of cancer cells [3]. Despite the importance of AuNPs within the field of nanomedicine, recent research has big concerns over the safety of using AuNPs in human clinical trials. AuNPs

shape and size is important factors regulating their interaction and toxicity with cells [4]. After administration, AuNPs are rapidly distributed in several tissues including blood, liver, spleen, kidney, brain, lung, heart, and stomach [5]. Intraperitoneal (i.p.) injection of 10 nm AuNPs produced hepatotoxic [6] and nephrotoxic effects in rats [7]. Also, 5 nm AuNPs induced DNA damage in a dose-dependent manner [8]. Additionally, the administration of 10 or 50 nm AuNPs induced an acute phase of proinflammatory cytokines in the cortex and medulla of rat kidneys [9]. AuNPs up-regulated Caspase-3, Caspase-8, and Caspase-9 gene expression [10], and decreased expression of Bcl-2 protein in osteosarcoma cells [4]. Other reports revealed no genotoxicity for 5 or 50 nm AuNPs on cell lines in vitro [11], or a decrease in cell viability [12].

Compared to other types of gold nanostructures, 50 nm nanorods (AuNRs) have a higher plasmonic photothermal effect due to the plasmon resonance absorption and scattering of light in the near-infrared region, and they are widely used in biomedical imaging, X-ray computed tomography (X-ray CT), for PTT and gene/drug delivery [13]. Injection of 50 nm AuNRs didn't produce any mortality or toxicity as indicated by animal behavior, gross morphology, blood biochemistry, hematological analysis, immunology, and histopathological examination in rats [14], rabbits [15], and pets [16]. On the other hand, when examined in vitro, 50 nm AuNRs have cytotoxic and genotoxic effects on mouse splenocytes and human normal and cancer cell lines in a dose-dependent manner [17]. The possibility that i.v. injection of 50 nm AuNRs can induce in vivo toxicity is still controversial. To date, large animal models haven't been previously examined for the possible toxicity following a single dose i.v. injection of 50 nm AuNRs. Therefore, this is the first study providing new insight into the acute and long-term acute toxicity of single i.v. injection of 75 µg of 50 nm AuNRs/kg in dogs based on hematological, serum biochemical analyses, light microscopy examination, immunohistochemical localization of caspase-3 and bcl-2 protein expression as a marker for apoptosis or antiapoptotic. Also, the viability of peripheral white blood cells (PWBCs) was evaluated using 3-(4,5-dimethylthiazol-2-yl)-2,5-diphenyltetrazolium bromide (MTT assay), and genotoxicity in PWBCs was determined using Comet assay.

Materials and methods

Chemicals

Unless otherwise mentioned all the chemicals used in the present study were purchased from Sigma-Aldrich (Sant-Louis, Missouri, USA).

Synthesis and characterization of 50 nm AuNRs

AuNRs solution was prepared using the seed-growth approach according to the method previously adopted [18]. Briefly, for the preparation of the seeding solution, 5 mL of 5×10^{-4} M $HAuCl_4$ was added to 5 mL, 2 of 10^{-1} M CTAB solution with gentle shaking, then 600 µL of 10^{-2} M ice-cold $NaBH_4$ was injected into the above mixture. The color of the mixture turned reddish-brown. For the preparation of the growth solution, 300 µL of 4×10^{-3} M $AgNO_3$ was added to a mixture of 5 mL of 2×10^{-1} M CTAB. To this aqueous mixture, 70 µL of 7.8×10^{-2} M ascorbic acid was added, and the color of the growth solution was changed from orange to colorless. Finally, 12 µL of the seed solution was injected into the growth solution. The color of the growth solution was changed slowly within 30-45 min to the reddish-purple. For the PEGylation of AuNRs, 0.05 g of thiol-terminated methoxy polyethylene glycol (mPEG-SH) of MW=5000 was added to the AuNRs solution. The mixture was kept overnight at room temperature. The raw nanorod solution twice by centrifugation at 15000 rpm for 20 min to pellet the nanorods, decanted, and then re-suspended to 10 ml of deionized water to remove excess CTAB and mPEG-SH. The absorption spectra of AuNRs solutions were determined by using a V-630 UV-VIS Spectrophotometer (Jasco, Japan). Transmission Electron Microscopic (TEM) images were obtained using JEOL JEM 2010 TEM operated at 200 kV accelerating voltage.

Animals

This work was conducted on eighteen mature native male dogs with an average of 2.31±0.45 years old, and 10.88+0.78 kg body weight. Dogs have been kept in dogs shelters and belong to the Egyptian Society for Mercy to Animals (ESMA, Egypt). Dogs were kept in separate cages; food was supplied three times daily, while water was offered *ad libtum*.

Experimental design

Experiment 1: Acute toxicity of i.v. injection of 75 µg 50 nm AuNRs/kg

In this experiment, control dogs (n=4), were i.v. injected with 10 ml of normal saline solution. For acute toxicity group (n=5): dogs were i.v. injected with a single dose of 75 µg of 50 nm AuNRs/kg body weight according to Abdoon et al. [16]. Dogs were observed for two weeks, and blood samples were collected from control and AuNRs injected dogs on day 3 and 14 after AuNRs injection for hematological and biochemical evaluation. Also, blood samples were collected on day 14 for evaluation of cytotoxicity and genotoxicity.

Experiment 2: Long-term acute toxicity study

Control animals (n=4) received i.v. injection of 1 ml/kg bodyweight saline solution, and in the long-term acute toxicity group (n=5): dogs were i.v injected with a single dose of 75 µg of 50 nm AuNRs/kg bodyweight, and animals were observed for 6 months. Blood samples were collected monthly from control and AuNRs injected dogs for hematological and biochemical evaluation and at the end of the experiment for cytotoxicity and genotoxicity evaluation.

In acute and long-term acute toxicity studies, dogs were examined daily for survival and any physiological, behavioral, or motor impairment.

Hematology and serum biochemical parameters

Blood samples were drawn from the Cephalic vein into an EDTA tube for routine hematology or into an anticoagulant-free tube for serum liver and kidney function analyses. Hematological Autoanalyzer (Exigo EOS Vet, SE-126 13 Stockholm, Sweden) was used to determine hematological parameters such as Red Blood Cell Count (RBC), White Blood Cell Count (WBC), Hemoglobin Concentration (HGB), Hematocrit (HCT), Mean Corpuscular Volume (MCV), Mean Corpuscular Hemoglobin (MCH), Mean Corpuscular Hemoglobin Concentration (MCHC), Red Blood Cell Distribution Width (RDW%), White Blood Cell Count (WBC), Lymphocytes (LYM), Monocytes (MON), Granulocytes (GRAN), and Platelets Counts (PLT).

Serum biochemical parameters for liver and kidney functions include Total Protein (TP), Albumin (ALB), Globulin (GLOB), Total Bilirubin (TBIL), Aspartate Transaminase (AST), Triglycerides

(TRG), Cholesterol (CHOL), Alkaline Phosphatase (ALK. Phos), Blood Urea Nitrogen (BUN), Uric Acid (UA), and creatinine (CREA) levels were estimated by using biochemical kits (Biomerieux, France) and UV spectrophotometer (Jenway, UK) as per the instruction manuals.

Liver, spleen, and kidney biopsy sampling

In the acute toxicity study, biopsy samples from the liver, spleen, and kidney were collected from the control (n=4) and experimental group (n=5) on day 14 after AuNRs injection. In the long term, biopsy samples from the liver, spleen, and kidney were collected from the control (n=4) and experimental group (n=5) at the end of the 6th month. Biopsy samples were used for histopathological and caspase-3 and bcl-2 protein expression.

In the two experiments, dogs were starved for 24 hours before laparotomy. On the day of the operation, dogs were injected i.m. with 1 ml ZylaJect for sedation (Adwaia Com., Egypt) followed by general anesthesia using i.v. injection of 10 mg/ml Propofol (Baxter, Caxton Way, Thetford, Norfolk, UK). Following anesthesia, the dog was placed on a surgical table, lying on his back. The abdominal hair was clipped over the abdomen; the skin was disinfected with surgical soap followed by ethanol and betadine, and a sterile drape was placed over the surgical site. Using a scalpel, an incision was made at the abdominal skin and peritoneum to open the abdominal cavity. The liver, spleen, and kidney were grossly evaluated for any change in size, morphology, texture, or presence of any focal pathological lesions, then biopsy samples were taken from these organs. Part of the biopsy sample was fixed in 10% formalin for histopathological examination, and the other part was fixed in 2.5% glutaraldehyde solution for electron microscopic evaluation. The abdominal incision was closed with one layer of self-dissolving sutures. The outer layer of the skin was closed with sutures. Animals were injected with long-acting antibiotics (Clamoxyl, Pfizer, Egypt) given intramuscularly for 7 days. Animals were carefully checked every day for 10 days after the operation.

Histopathology examination

For control, acute, and long-term acute studies, biopsy samples from the kidney, liver, and spleen were fixed in 10% formalin solution for 48 h, then dehydrated in graded alcohol (50%, 70%, 80%, 90%, and 100%), cleared in xylene and embedded in paraffin blocks. Sections (5 µm) were cut with a rotary microtome, stained with hematoxylin-eosin, and observed under a bright-field microscope (Olympus, Japan). All samples were examined by the same operator and photographs were captured with a CCD camera Olympus DP12 attached to the microscope. Scoring of histopathologic changes has been done semi-quantitively applying the ordinal method. To avoid bias, all the histopathological examinations were conducted by the same person.

Immunostaining for caspase-3 protein expression

The second section from the same block was deparaffinized, rehydrated, and immunostained using Caspase 3 (CPP32) Ab-4 primary rabbit polyclonal antibody (Thermo Scientific) according to Virkajarvi et al. [19]; to assess cellular apoptosis; to assess antiapoptotic activity. The section was pre-treated using a pressure cooker heat-mediated antigen retrieval with sodium citrate buffer (pH6) for 30 minutes and incubated overnight at +4°C with primary antibody at 1/1000 dilution. An HRP-conjugated secondary (1/10000 dilution) was used to detect the primary for 1hr at room temperature. DAB was used as chromogen, diluted 1/100 and incubated for 10 min at room temperature. The section was counterstained with hematoxylin and mounted with DPX. The sections were examined under an Olympus research microscope with an attached CCD digital camera Olympus SC-100. Digital photomicrographic sections were taken at various magnifications.

Peripheral white blood cell viability assay

The effect of nano-gold on the viability of peripheral white blood cells was determined by measuring the capacity of reducing enzymes present in viable cells to convert MTT to formazan crystals. Briefly, PWBCs from control, acute, long-term acute toxicity groups were incubated in cell culture plates at 37°C under a 5% CO_2 humidified air, the media were removed and 100 µL of serum-free media containing 1.2 mM of MTT dissolved in phosphate-buffered-saline (PBS), pH 7.4, was added to each well. After 2 h incubation in a CO_2 incubator at 37°C, the media were then decanted off by inverting the plate, and 100 µL of isopropyl alcohol was added to each well, with shaking for 1 h to dissolve the formazan crystals. The color intensity of the blue formazan solution formed in each well was measured at a wavelength of 550 nm using a microplate reader (EL 312e, BIO-TEK, Winooski, VT, USA). The percentage of cell viability was calculated relative to control wells designated as 100% viable cells.

Peripheral blood Comet assay

Blood samples were collected on days (Acute toxicity) and after 6 months (Long-term toxicity) of AuNRs injection, then PWBCs were separated by density gradient separation using Histopaque according to the manufacturers. % DNA fragmentation was checked using the alkaline version of the Comet Assay as described by Schlörmann and Glei [20].

Comets were examined at 400X magnification using a fluorescent microscope with an image analysis system (Perceptive Instruments Comet assay V2, Instem, Great Shelford Cambridge, CB22 5LD, UK). Sixty cells per slide were scored and recorded for each animal. The mean values ± SE for the percentage of DNA in the tail, tail length (µm), and tail moment were recorded.

Statistical analysis

Results were expressed as mean ± standard error of the mean (SEM). Statistical analysis was performed using the SPSS (v16 software; IBM Corporation, Somers, NY, USA). For blood profile and biochemistry, morphometric and genotoxicity analysis One-way Analysis of Variance (ANOVA) followed by Tukey's test was used. *P<0.05 and **P<0.01 were considered statistically significant.

Results

Characterization of AuNRs

TEM images showed AuNRs with homogenized rod shape (Figure 1A), with an average size of 50.8±7.2 nm length 10.3±1.4 nm width, and 4.9 aspect ratio were synthesized. A strong absorption band with a maximum at ~808 nm resulting from the electronic oscillation of the electrons of the nanorod along its long axis and a weak band at ~530nm polarized resulting from nanorod electrons oscillations along the short axis of the nanorod (Figure 1B).

Animal behavior after AuNRs injection

There were no major clinical changes in eating, drinking

behavior, defecation, urination, or unusual symptoms after i.v. injection of 75 µg of 50 nm AuNRs/kg bodyweight in acute or long-term acute toxicity groups when compared with the control one.

Hematology profile

Selected standard hematology markers such as RBCs count, HCT, MCV, HGB, MCH, MCHC values, PLTs, WBCs, NEU, GRA, and LYM count, all are presented in Table 1. Results indicated that under acute toxicity study, i.v. injection of 50 nm AuNRs significantly decreases ($P<0.05$) MCV, WBCs, LYM, and PLTs count, and increases ($P<0.05$) the number of when compared with control animals. Meanwhile, in long-term acute toxicity study, i.v. injection of 50 nm AuNRs significantly decreased ($P<0.05$) the RBCs count, HCT, HGB, LYM, and PLTs count, while it significantly increased ($P<0.05$) the number of GRA as compared with the control dogs.

Liver and kidney functions

By measuring a variety of biochemical factors in the blood serum, it is possible to assess liver and kidney functions. As shown in Table 2, the biochemistry results of the 50 nm AuNRs treated dogs comprising TP, ALB, GLOB, TBIL, AST, TRG, CHOL, ALK-Ph, BUN, UA, and CREA levels were reported. Under acute toxicity experiment, i.v. injection of 50 nm AuNRs significantly increases ($P<0.05$) TP, GLOB, AST, and CREA concentrations when compared with the control non-treated group. ALK-Phos significantly ($P<0.05$) higher in control than AuNRs injected dogs. In addition, in long-term toxicity, i.v. injection of AuNRs significantly increases ($P<0.05$) TP, GLOB, and CREA concentrations when compared with the control group. ALK-Phos and CHOL concentrations were significantly ($P<0.05$) higher in control non-treated than AuNRs injected dogs.

Histopathology

Compared with control dogs, no gross morphological changes or lesions were detected in the kidney, liver, or spleen of acute AuNRs injected dogs (Day 14) or long-term acute toxicity (six months) AuNRs injected dogs. The histopathological changes in the renal, hepatic, and splenic tissues of dogs i.v. injected with 50 nm AuNRs are presented in Figure 2. In the acute toxicity study, compared with control animals (Figure 2A), histopathological examination of the renal tissue of AuNRs injected dogs showed an intact preserved cellular architecture similar to the control animals (Figure 2B). However, under long-term acute toxicity experiment, single i.v. injection of 50 nm AuNRs produced severe histopathological changes. The epithelial lining of renal collecting tubules showed mild cloudy swelling and focal vacuolar degeneration. RBCs and hyaline casts were also seen within the lumen of renal collecting tubules. Renal collecting tubules showed partial sloughing of their lining epithelium (Figure 2C). Histology of hepatic tissue demonstrated normal morphometry of hepatocytes and hepatic portal area in control (Figure 2D) and acute toxicity groups, but mild lymphocytic infiltration was noticed within sinusoids of the acute AuNRs injected dogs (Figure 2E). On the other hand, in the long-term AuNRs injected dogs, the hepatocytes showed mild cytoplasmic hydropic degeneration. Intralobular focal aggregates inflammatory cells formed mainly of small mature lymphocytes and polymorphs. At the periphery of the hepatic lobules, short fibrous tissue septae harboring few inflammatory cells were recorded (Figure 2F). Histopathological examination of the splenic tissue in acute toxicity study showed an intact preserved architecture similar to the control animals (Figure 2G). White pulp showed lymphoid follicles with prominent spiral arterioles with prominent central arterioles and surrounding congested red pulp (Figure 2H), while it showed marked congestion in the long-term acute toxicity study (Figure 2I).

Immunostaining for caspase-3 protein expression

Caspase-3 enzymes play an important role in cell death. Protein expression for the caspase-3 gene was significantly ($P<0.05$) higher in the kidney of the acute toxicity group and long-term acute toxicity group as compared to the control group (Figure 3A, B, and C). It showed that the optical density of caspase-3 immunostaining in the liver significantly increased ($P<0.05$) in acute toxicity and long-term acute toxicity groups as compared to the control group (Figure 3D, E, and F) for control, acute and long-term toxicity, respectively). Also, the spleen optical density increased significantly ($P<0.05$) in the acute toxicity group and long-term acute toxicity group as compared to the control one (Figure 3G, H, and I).

Cell viability

The effect of i.v. injection of a single dose of 50 nm AuNRs on the viability of peripheral white blood cells is demonstrated in Table 3. Analysis of data revealed that i.v. injection of a single dose of 50nm AuNRs either in acute or long-term acute toxicity studies significantly decreased ($P<0.01$) viability of PWBCs when compared with the control group.

Comet assay

The effect of i.v. injection of 50nm AuNRs on comet assay (DNA fragmentation, tail length, and tail moment) and cell viability is presented in Table 4 and Figure 5. Results indicated that i.v. injection of 50 nm AuNRs significantly increases ($P<0.01$) tail length, tail moment, and %DNA fragmentation in both acute and long-term-acute toxicity groups when compared with control one (Figure 5A, B for control and AuNRs injected group, respectively).

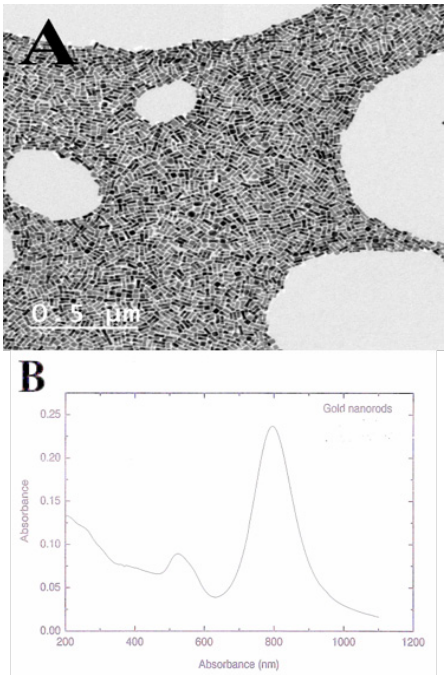

Figure 1: Characterization of AuNRs. **A**: TEM micrograph image for 50 nm AuNRs (Bar 200 nm). **B**: Absorption spectra of the synthesized AuNRs.

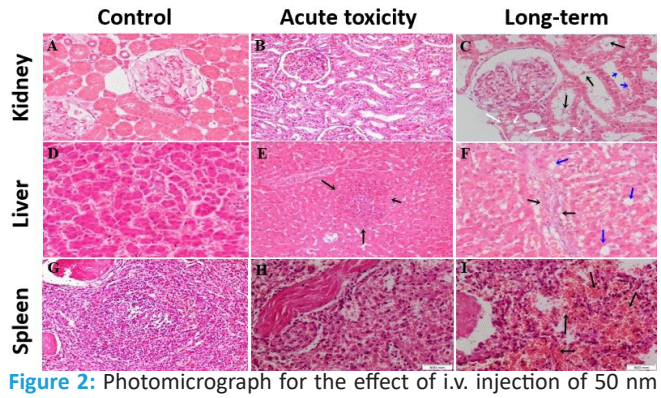

Figure 2: Photomicrograph for the effect of i.v. injection of 50 nm AuNRs showing a preserved structure of renal tissue **(A)** control with ordinary glomeruli and ordinary tubules lined by low cuboidal epithelium; **(B)** acute toxicity similar to control; and **(C)** long-term acute toxicity showed mild vacuolar degeneration (White arrows) and mild cloudy swelling (Blue arrows) within tubular lining epithelium, RBC casts and hyaline casts within the lumina of collecting tubules (Black arrow). Photomicrograph for the effect of i.v. injection of 50 nm AuNRs showing a preserved structure of hepatic tissue in control with ordinary hepatocytes arranged in single cell thick plates **(D)** and acute toxicity with mild inflammatory cellular infiltrate formed mainly of small mature lymphocytes and polymorphs (Black arrows) **(E)**, and long-term acute toxicity with moderate fibrous tissue expansion of some portal tracts showing extending fibrous tissue septae (Black arrows) entangling inflammatory cells together with vacuolation and mild hydropic degeneration within scattered hepatocytes **(F)** Photomicrograph for the effect of i.v. injection of 50 nm AuNRs showing a preserved architecture of splenic tissue in control **(G)** showing white pulp lymphoid follicles with prominent spiral arterioles, and acute toxicity with mild congestion within red pulp and fibrous tissue septae (Black arrows) with some inflammatory cells (White arrows) **(H)**, and long-term acute toxicity with marked congestion within red pulp the effect of i.v. injection of 50 nm AuNRs showing a preserved architecture of splenic tissue (Black arrows) **(I)** (H&E 200x).

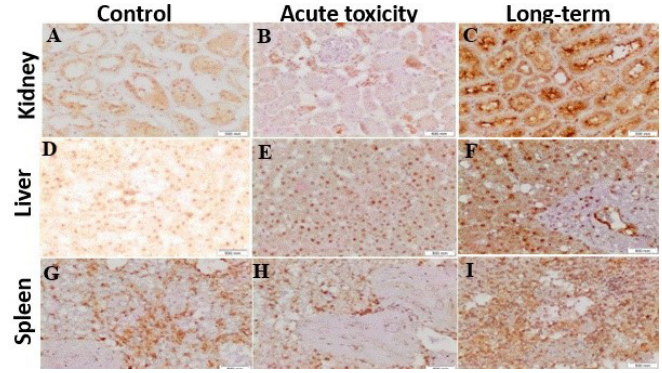

Figure 3: Photomicrograph showing immunohistochemical staining of Caspase-3 in the kidney (**A**, **B**, and **C**); spleen (**D**, **E**, and **F**) and liver (G, H, and I) for control, acute, and long-term toxicity, respectively, of i.v. injection of 50 nm AuNRs in dogs.

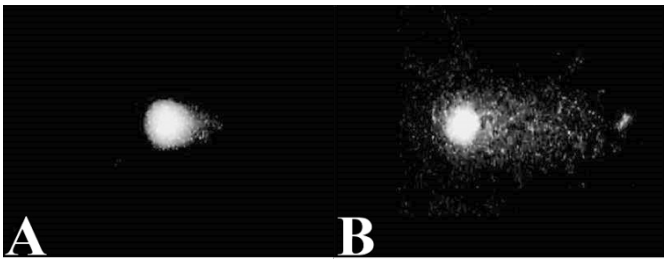

Figure 4: Micrograph showing Comet assy for control **(A)** and PEBcs from 50 nm AuNRs injected dogs **(B)**.

Table 1: Effect of i.v. injection of a single dose of 50 nm AuNRs on blood profile in acute and long-term toxicity in dogs (Mean S.E.)

Blood parameter	Acute toxicity				Long-term acute toxicity											
	Day-3		Day-14		1st Month		2nd Month		3rd Month		4th Month		5th Month		6th Month	
	Cont	AuNR	Cont.	AuNR	Cont	AuNR	Cont	AuNR	Cont	AuNR	Cont	AuNR	Cont	AuNR	Cont	AuNR
RBC (10^6/µL)	6.0 ±0.4	6.4 ±0.4	7.0 ±0.2	6.9 ±0.2	6.6 ±0.7	6.5 ±0.5	6.2 ±0.3	6.6 ±0.4	6.5 ±0.2	6.5 ±0.3	8.3 ±0.5*	7.2 ±0.3	7.5 ±0.2*	6.6 ±0.2	7.9 ±0.1*	7.2 ±0.3
HCT (%)	45.4 ±1.9	45.4 ±1.6	43.7 ±1.5	46.0 ±1.3	47.6 ±1.5	45.4 ±1.3	43.4 ±1.3	45.3 ±1.0	42.9 ±1.7	41.5 ±1.4	51.8 ±1.6*	44.5 ±0.9	46.2 ±1.1*	41.1 ±1.6	46.3 ±1.0*	42.1 ±1.8
HGB (g/dL)	14.5 ±0.1	14.5 ±0.5	14.8 ±0.4	15.7 ±0.5	15.3 ±0.7	14.6 ±0.3	13.9 ±1.0	14.8 ±0.9	14.5 ±0.6	14.1 ±0.5	18.3 ±0.3*	15.6 ±0.6	16.4 ±0.7*	14.7 ±0.6	15.8 ±0.4	15.4 ±0.6
MCV (µm³)	71.1 ±1.4	71.1 ±1.3	66.5 ±1.8*	62.1 ±0.8	73.1 ±1.8	70.2 ±1.1	69.8 ±1.7	68.6 ±1.3	64.9 ±1.4	63.8 ±1.0	62.1 ±1.5	61.7 ±1.7	62.4 ±1.7	59.7 ±1.6	58.7 ±1.4	58.4 ±1.3
MCH (pg)	23.2 ±0.4	23.2 ±0.4	21.0 ±0.4	22.7 ±0.1*	23.5 ±0.2*	22.4 ±0.2	22.3 ±0.3	22.5 ±0.2	22.0 ±0.2	21.7 ±0.1	22.1 ±0.3	21.3 ±0.2	21.3 ±0.3	21.3 ±0.2	21.3 ±0.2	21.4 ±0.2
MCHC (g/dL)	32.5 ±0.3	32.5 ±0.2	33.5 ±0.8	34.1 ±0.4	32.1 ±0.6	31.6 ±0.4	32.0 ±0.4	32.9 ±0.4	33.4 ±0.6	34.1 ±0.2	35.6 ±0.2*	34.5 ±0.2	34.2 ±0.6	35.4 ±0.4	36.3 ±0.4	36.7 ±0.5
RDW (%)	22.1 ±0.4	22.4 ±0.4	22.7 ±0.5	22.1 ±0.4	23.2 ±0.3	23.6 ±0.3	22.8 ±0.3	23.0 ±0.2	22.0 ±0.4	22.6 ±0.5	21.2 ±0.6	22.3 ±0.5	21.6 ±0.4	22.0 ±0.7	23.5 ±0.7	23.0 ±0.6
RDWa	58.4± 1.6	58.0 ±1.0	49.3 ±1.5	51.4 ±1.8	62.7 ±1.2	59.5 ±1.6	57.5 ±1.0	56.3 ±1.4	50.5 ±1.3	49.9 ±1.5	45.0 ±1.0	46.3 ±1.9	46.6 ±1.7	44.0 ±1.6	45.3 ±1.5	43.7 ±2.0
WBC (10^3/µL)	19.0± 0.7*	16.4 ±0.6	18.0 ±0.8*	15.8 ±0.4	16.9 ±0.6	15.9 ±0.1	18.8 ±0.7	17.0 ±0.3	17.5 ±0.2	13.3 ±0.4	15.8 ±0.3*	13.5 ±0.5	18.3 ±0.9	18.3 ±0.5	16.1 ±0.5	16.8 ±0.9
LYM (%)	33.0± 1.9	24.4 ±1.8*	30.6 ±1.5	32.1 ±1.3	34.1 ±1.0	32.3 ±1.9	31.8 ±1.1	30.0 ±1.4	22.3 ±1.3	27.3 ±1.5*	27.6 ±1.2	31.4 ±1.4*	26.5 ±1.3	32.7 ±1.5*	29.0 ±1.2	32.2 ±1.2*
MON (%)	11.9± 0.1*	10.3 ±0.3	11.5 ±0.6	11.1 ±0.8	11.1 ±0.4	13.7 ±0.7*	11.9 ±0.5	11.4 ±0.5	9.3 ±0.3	11.1 ±0.6*	12.2 ±0.2	11.7 ±0.3	12.7 ±0.9	10.2 ±0.8	13.4 ±0.3	12.9 ±0.5
GRAN (%)	56.6± 0.6	64.1 ±1.4*	56.8 ±0.5	66.8 ±0.7*	56.8 ±0.2	55.4 ±0.8	56.3 ±0.2	58.7 ±0.5*	61.6 ±0.5	66.9 ±0.6*	56.9 ±0.6	60.2 ±0.2*	54.4 ±0.4	63.3 ±0.5*	53.5 ±0.6	58.1 ±0.4*

PLT (10^3/µL)	264.2± 12.2*	238.0± 12.0	254.6 ±12.3	253.9 ±18.6	266.6 ±15.7	254.2 ±15.6	204.4 ±20.9	224.2 ±18.8	259.6 ±20.0	255.5 ±16.9	274.0 ±12.1	312.8 ±12.0	233.8 ±29.4	250.3 ±26.7	373.0 ±9.4*	317.3 ±7.5
MPV (µm³)	8.4± 0.6	9.0± 0.3	7.6 ±0.9	8.4 ±0.8	9.22 ±0.7	10.0 ±0.5	9.3 ±0.1	8.8 ±0.4	8.3 ±0.9	8.5 ±0.9	8.9 ±0.3	7.8 ±0.8	7.8 ±0.8	7.2 ±0.6	7.3 ±0.9	7.8 ±0.6

RBC: Red Blood Cells Count; WBC: White Blood Cells Count; HGB: Hemoglobin Concentration; HCT: Hematocrit; MCV: Mean Corpuscular Volume; MCH: Mean Corpuscular Hemoglobin; MCHC: Mean Corpuscular Hemoglobin Concentration; RDW%: Red Blood Cell Distribution Width; WBC: White Blood Cell Count; LYM Lymphocytes; MON Monocytes; GRAN: Granulocytes; PLT: Platelets Counts; And MPA: Mean Platelets Volume.

Table 2: Effect of i.v. injection of a single dose of 50 nm AuNRs on liver and kidney functions in acute and long-term toxicity in dogs (Mean S.E.).

Item	Acute toxicity				Long-term acute toxicity											
	Day-3		Day-14		1st Month		2nd Month		3rd Month		4th Month		5th Month		6th Month	
	Cont	AuNRs	Cont	AuNR	Cont	AuNR	Cont	AuNR	Cont	AuNR	Cont	AuNR	Cont	AuNR	Cont	AuNR
TPg/dl	6.2± 0.4	7.1± 0.2*	6.4± 0.2	6.6± 0.5	6.6± 0.6	6.3± 0.3	6.1± 0.5	6.5± 0.1	7.1± 0.6	7.0± 0.5	7.7± 0.2	7.1± 0.3	6.9± 0.1	8.4± 0.4*	7.4± 0.6	6.8± 0.2
Alb g/dl	3.3± 0.1	3.6± 0.4	3.5± 0.4	3.5± 0.2	3.4± 0.3	3.2± 0.3	3.5± 0.4	4.1± 0.2	4.1± 0.4	4.5± 0.5	4.2± 0.1	3.9± 0.2	4.2± 0.1	4.4± 0.2	4.3± 0.4	3.9± 0.1
Glob g/dl	2.9± 0.2	3.5± 0.3*	2.9± 0.3	3.1± 0.2	3.2± 0.4	3.1± 0.2	2.6± 0.4	2.4± 0.2	3.0± 0.4	2.5± 0.1	3.5± 0.2	3.2± 0.4	2.7± 0.2	4.0± 0.4*	3.1± 0.2	2.9± 0.1
AST (U/L)	16.2± 0.2	16.8± 0.3	18.8± 0.3	21.7 ±0.2*	16.6± 0.7*	17.7 ±0.8	16.2± 1.5	16.8± 1.3	14.6± 1.1	15.2± 1.0	15.8± 1.1	14.2± 0.8	17.2± 0.8	17.2± 0.6	17.0± 0.4	17.8± 0.7
Alk.Ph U/L	73.4± 3.6*	49.9± 5.5	74.5± 3.1	76.7± 2.2	108.4± 10.3	105.2± 6.9	100.9 ±8.7	111.1 ±3.7	100.4 ±7.2	100.1 ±9.9	116.2 ±4.6	120.7± 6.4	118.0 ±5.4*	102.3 ±5.1	122.4 ±6.2*	97.4± 2.3
Choles	6.4± 0.2	6.0± 0.4	4.9± 0.9	4.2± 0.5	6.2± 0.3*	5.1± 0.2	17.1± 0.5*	10.6± 1.1	21.2± 1.4	21.5± 1.3	21.6± 0.8	21.7± 0.8	17.1± 0.3	17.0± 0.7	26.6± 0.6	25.4± 0.8
Trigly	0.4± 0.1	0.3± 0.1	0.8± 0.1	0.5± 0.1	0.5± 0.1	0.4± 0.1	0.5± 0.1	0.4± 0.1	0.3± 0.1	0.4± 0.02	0.4± 0.1	0.4± 0.1	0.5± 0.1	0.4± 0.1	0.9± 0.1	0.5± 0.1
Bilirub	0.3± 0.1	0.2± 0.1	0.3± 0.1	0.2± 0.1	0.3± 0.1	0.3± 0.1	0.3± 0.1	0.4± 0.1	0.7± 0.1	0.6± 0.1	0.5± 0.1	0.7± 0.1*	0.5± 0.1	0.7±0.1*	0.6± 0.2	0.5± 0.1
BUN Mg/dl	47.2± 0.2	48.4± 0.6	49.4± 0.3	49.0± 0.5	33.9 0.6	33.2± 0.9	45.0± 0.5*	39.9± 0.5	47.9± 0.6	48.5± 0.5	47.0± 0.9	46.3± 0.5	46.5± 0.7	49.0± 0.2*	48.8± 0.4	49.2± 0.4
UA mg/dl	3.3± 0.4	3.2± 0.5	3.0± 0.6	3.1± 0.5	2.2± 0.4	2.3± 0.3	2.5± 0.3	3.0± 0.2	3.2± 0.2	3.6± 0.4	4.0± 0.3	4.0± 0.3	3.0± 0.3	3.4± 0.2	3.1± 0.3	3.4± 0.6
Creat mg/dl	12.9± 0.6	12.1± 0.9	18.0± 0.5	23.2± 0.4*	8.4± 0.9	8.8± 0.6	19.4± 0.4	19.5± 0.3	17.9± 0.7	16.9± 0.5	42.5± 0.3	42.2± 0.2	31.7± 0.9	39.6± 0.8*	24.1± 0.7	33.4± 0.9*

*P<0.05

Table 3: Effect of i.v. injection of a single dose of 50 nm AuNRs on Caspase-3 protein expression (Optical density) in acute and long-term toxicity in dogs (Mean S.E.).

Group / Tissue	Liver	Kidney	Spleen
Control	0.33±0.04	0.35±0.01	0.33±0.02
Acute Toxicity	0.44±0.03*	0.57±0.02*	0.61±0.01*
Long Term Toxicity	0.48±0.02*	0.41±0.02*	0.51±0.03*

* Differ significantly within the same column at p<0.05

Table 4: Effect of i.v. injection of a single dose of 50 nm AuNRs on Caspase-3 protein expression (Area percentage) in acute and long-term toxicity in dogs (Mean S.E.).

Group / Tissue	Liver	Kidney	Spleen
Control	0.92±0.05	1.41±0.21	1.1±0.19
Acute Toxicity	1.16± 0.13*	1.46± 0.21	2.56±0.44*
Long Term Toxicity	1.16± 0.13*	1.45± 0.54	3.37±0.57*

* Differ significantly within the same column at p<0.05

Table 5: Effect of i.v. injection of a single dose of 50 nm AuNRs on the viability of PWBCs in control, acute and long-tern toxicity in dogs.

Group	% Cell viability (Mean ± SE)
Control -ve	88.04±0.25
Acute toxicity	83.68±0.45**
Long-term acute toxicity	82.6±0.37**

* Differ significantly within the same column at p<0.01

Table 6: Effect of i.v. injection of a single dose of 50 nm AuNRs on Comet analysis (% of DNA fragmentation, Comet tail length, and Comet tail moment) in control, acute and long-term toxicity in dogs.

Group	Comet assay		
	Tail Length (µm, Mean±SE)	Tail Moment (Mean±SE)	% DNA fragmentation (Mean±SE)
Control -ve	2.14±0.09	0.19±0.05	3.66±0.20
Acute toxicity	11.35±0.22**	3.17±0.04**	7.12±0.63**
Long-term acute toxicity	12.20±0.23**	4.22±0.07**	7.25±0.75**

* Differ significantly within the same column at p<0.01

Discussion

Gold nanorods (AuNRs) offer an excellent opportunity for biomedical and industrial applications, They're utilized in PTT, and drug/gene delivery, as novel diagnostic, and therapeutic approaches in cancer. Currently, the available data on the toxicity of AuNRs were examined in vivo and were conducted on small lab animals. Though results might not predict the in vivo toxicity accurately.

In the present work, results showed that in both acute and long-term acute toxicity studies, no behavioral changes were recorded after i.v. injection 50 nm AuNRs in dogs. All physiological functions including feeding, drinking, urination, defecation, motor, and sensing functions were similar between the control and 50 nm AuNRs injected dogs. These results indicated that the i.v. injection of 50 nm AuNRs did not produce any apparent toxicity in dogs. Similar results were recorded in rats [14,21], rabbits [15], and pets [16]. On the contrary, after direct exposure to naked colloidal 8 to 37 nm AuNPs, a high percentage of the mice showed loss of weight and appetite and died within 21 days [22]. Also, food and water intake were changed after inhalation of nm AuNPs in rats [23]. This difference could be related to the shape, surface chemistry, or route of administration of AuNPs.

Furthermore, in this work, no gross morphological changes or signs of inflammation or damage were detected in the hepatic, splenic, and renal tissues of 50 nm AuNRs injected dogs either in acute or long-term acute toxicity studies. Additionally, histopathological examination of biopsy samples collected on Day 14 after 50 nm AuNRs injection (acute toxicity study) revealed that the architecture of renal, hepatic, and splenic tissues was similar in control and acute 50 nm AuNRs injected dogs, only some aggregations of lymphocytes were detected within the hepatic tissues of 50 nm AuNRs injected dogs. However, the histology of splenic tissue of 50 nm AuNRs injected dogs showed mild to moderate congestion when compared with control dogs. Congestion might have resulted from the leakage of lysosomal hydrolytic enzymes that leads to cytoplasmic degeneration and macromolecular crowding [24]. In addition, biopsy samples collected from long-term acute toxicity experiments showed some histopathological changes. In long-term acute toxicity, the lumen of the renal collecting tubules showed moderate hyaline casts, and the lining epithelium showed cloudy swelling, vacuolar degeneration, and sloughing of epithelial lining into the lumen. The cloudy swelling might have been initiated as a result of disturbances of membrane function that led to a massive influx of water and Na^{+}. An increase in intracellular water leads to renal injury by AuNRs [25]. In a long-term acute toxicity study, the liver of the 50 nm AuNRs injected group showed signs of intralobular focal aggregation of inflammatory cells, formed mainly of small mature lymphocytes and polymorphs, thin fibrous tissue septae were also seen at the periphery of the lobules, hepatocytes showed mild hydropic degeneration. Also, the presence of lymphocytic infiltrations in both acute and long-term acute toxicity might suggest that 50 nm AuNRs could interact with proteins and enzymes of the hepatic tissue and interfere with the antioxidant defense mechanism, leading to ROS generation which in turn might initiate an inflammatory response [26]. Similarly, AuNPs produced hepatotoxicity and nephrotoxicity in rats and mice [9,27]. Apoptosis and inflammation of liver tissue were detected in mice after i.v. injection of 10 nm AuNPs and potentially induce long-term organ damage and toxicity [28]. The mechanism by which AuNRs could induce nephrotoxicity or hepatotoxicity remains unknown. ROS produced by AuNPs might induce cellular damage by destructing the proteins, DNA, membranes, and other organelles like mitochondria, and nucleus [29]. In contrast, some reports have indicated that 50 nm AuNRs showed no hepatotoxicity or nephrotoxicity in rats [14,30], rabbits [15], and pets [16]. This difference might be due to the route of administration, duration of exposure, or species difference.

Moreover, blood cells could be more sensitive to AuNR because it is administered intravenously. Complete blood count indicated that i.v. injection of 50 nm AuNRs induced a significant ($P<0.05$) decrease in RBCs, HCT, and HGB values at the long-term acute toxicity level when compared with control animals. Also, lymphocytes and granulocytes were higher ($P<0.05$) in 50 nm AuNRs injected dogs compared with control one. These results may indicate that i.v. injection of 50 nm AuNRs could induce blood hemolysis leading to a decrease in the number of RBCs, HCT, and HGB. In accordance, AuNPs decrease the number of red blood cells, HGB, and HCT values after i.v. injection in rats [31] and mice [32]. The CTAB-AuNRs induced blood hemolysis through the Ca^{2+} pathway due to the circulating unbound CTAB residues [33]. In contrast, hematological parameters were not affected by i.v. injection of 10 nm AuNPs in rats [28,34]. This contradiction could be due to species differences in the pharmacokinetics of AuNPs, or it could be due to differences in shape, size, dose, or time of exposure to AuNPs.

Meanwhile, serum levels of total protein, globulin (in acute and long-term acute toxicity studies and AST (in acute toxicity) were higher ($P<0.05$), and creatinine level was higher ($P<0.05$) in both acute and long-term-acute toxicity groups when compared with the control one. Similarly, AuNPs could alter some blood biochemical parameters in mice [35], and rats [36]. Hepatic damage is associated with the release of liver enzymes into the circulation [37]. Also, nephrotoxicity was recorded after i.v. injection of AgNPs in rats, this was associated with higher values of urea, creatinine, and uric acid when compared with the control one [38]. AuNPs are relatively difficult to biodegrade and therefore might accumulate in organs/tissues for a longer period or permanently and produce their hepatotoxic and nephrotoxic effects [39], or it could be due to the toxic effect of CTAB residues in blood. On the contrary, no significant differences in hematological or serum biochemical values were detected after intratumoral injection of AuNPs in pets indicating the safety of using AuNRs [16], or in rats [14,34]. This discrepancy may be due, in part, to different preparations, surface coatings, and model systems, or because of the route of AuNPs injection.

Furthermore, in the present study, i.v. injection of a single dose of 50 nm AuNRs significantly ($P<0.05$) increased Caspase-3 protein expression in the spleen, and kidney in both acute and long-term acute toxicity experiments. AuNPs toxicity might increase pro-inflammatory cytokines and activation of pro-inflammatory cells leading to increased ROS production [40]. These results are corroborated by previous findings [41,42]. Caspases are responsible for the induction of apoptosis and cell death, activation of *caspase-3* was associated with the downregulation of antiapoptotic genes such as *bcl2* and upregulation of apoptotic markers including *Bax* and *p53* genes. All these events contribute to the development of the morphological signs of apoptosis [41].

Furthermore, compared with the control group, i.v. injection of 75 µg of 50 nm AuNRs/kg body weight significantly ($P<0.05$)

decreased the viability of PWBCs in both acute and long-term acute toxicity in dogs. Also, AuNRs significantly ($P<0.01$) increase the percentages of DNA fragmentation, tail length, and tail moment in PWBCs. These results are concomitant to previous studies in which the injection of AuNPs was genotoxic when injected in rats [42,43]. Also, 50 nm AuNRs or AuNPs induced a genotoxic effect when incubated with human PWBCs or in vitro using different cell lines or PWBCs [44,45]. The mechanism underlying the cytotoxic and genotoxic effects of AuNRs is still unknown. ROS-induced oxidative DNA damage might be one of the mechanisms by which AuNPs could produce a genotoxic effect. AuNPs induced their cytotoxic and genotoxic effect through the imbalance of cellular redox by inhibition of thioredoxin reductase enzyme, which in turn leads to mitochondrial dysfunction and induction of apoptosis [46]. In contrast, 50 nm AuNPs failed to induce DNA fragmentation in cell lines in vitro [34,47]. Lebedova et al. [11] reported that 50 nm AuNPs increased cell viability of human bronchial cell lines, and it had no genotoxic effect when compared with control. These discrepancies could be due to the duration of exposure, the experimental design (animal models or in vitro studies), doses applied, the route of administration), and the use of different sizes and types of AuNPs.

Conclusion

I.v. injection of 50 nm AuNRs did not elicit morphological changes, however, it could induce histopathological, some hematological, and blood biochemical changes related to liver and kidney functions and decrease in viability and increase DNA fragmentation of PWBCs, under acute and long-term acute toxicity studies. Based on this profile, i.v. injection of 50 nm AuNRs is not the proper route for administration in dogs.

Declarations

Conflict of interest: The authors report no conflicts of interest in this work.

Funding: The authors gratefully acknowledge the financial support provided by Misr El-Kheir Foundation to conduct this work (Proj ID: LGA 03 15 0032, entitled Applications of photothermal therapy using gold nanoparticles in cancer, PI: Prof Ahmed S. Abdoon).

Author contributions: ASSA&KH designed the experiments, ASSA, AAGE, KOM, EA, BA performed the experiments. ASSA, KH, AMS, and AHS analyzed the data. ASSA wrote the manuscript. All authors were involved in editing the final manuscript and approved its final form.

Acknowledgment: We gratefully acknowledge Mrs. Mona Khalil for her kind support in conducting this work at the dog shelter that belongs to the Egyptian Society for Merci of Animals (ESMA, Egypt). We also thank Prof. Mona Abou Zeid for her great help in the Comet assay work.

Availability of data and materials: All data generated or analyzed during this study were included in the article.

Ethical approval: Animals were kept and handled according to the Guide for the Care and use of Laboratory Animals, and the study was approved by the Scientific Committee at the Veterinary Research Division and the Ethical Committee for Medical Research at the National Research Centre of Egypt.

Consent to participate: Not applicable.

Consent for publication: Not applicable.

References

1. Kabir T, Rahman H, Akter R, et al. Potential role of curcumin and its nanoformulations to treat various types of cancers. Biomolecules. 2021; 11: 392.
2. Singh V, Kumar K, Purohit P, et al. Exploration of therapeutic applicability and different signaling mechanism of various phytopharmacological agents for treatment of breast cancer. Biomed Pharmacother. 2021; 139: 111584.
3. Jain S, Hirst DG, O'Sullivan JM. Gold nanoparticles as novel agents for cancer therapy. Br J Radiol. 2012; 85: 101-113.
4. Steckiewicz KP, Barcinska E, Malankowska A, et al. Impact of gold nanoparticles shape on their cytotoxicity against human osteoblast and osteosarcoma in in vitro model. Evaluation of the safety of use and anti-cancer potential. J. Mater. Sci. Mater. Med. 2019; 30: 22.
5. Bailly AL, Correard F, Popov A, et al. In vivo evaluation of safety, biodistribution and pharmacokinetics of laser-synthesized gold nanoparticles. Scientific Reports. 2019; 9: 12890.
6. Abdelhalim MAK, Moussa SAA, Qaid HAY, et al. Potential effects of different natural antioxidants on inflammatory damage and oxidative-mediated hepatotoxicity induced by gold nanoparticles. Int J Nanomedicine. 2018; 13: 7931-7938.
7. Abdelhalim MAK, Qaid HA, Al-Mohy Y, et al. Effects of quercetin and arginine on the nephrotoxicity and lipid peroxidation induced by gold nanoparticles in vivo. Int J Nanomedicine. 2018; 13: 7765-7770.
8. Zarska M, Sramek M, Novotny F, et al. Biological safety and tissue distribution of (16-mercaptohexadecyl) trimethylammonium bromide-modified cationic gold nanorods. Biomaterials. 2018; 154: 275-290.
9. Khan HA, Ibrahim KE, Khan A, et al. Immunostaining of proinflammatory cytokines in renal cortex and medulla of rats exposed to gold nanoparticles. Histol Histopathol. 2017; 32: 597-607.
10. Arshad M, Ozaslan M, Ali HK, et al. Molecular investigation of gold nanoparticles toxicity in mice model and p53 Activation. Journal of Biological Sciences. 2019; 19: 391-395.
11. Lebedová J, Hedberg YS, Wallinder OI, et al. (2018) Size-dependent genotoxicity of silver, gold and platinum nanoparticles studied using the mini-gel comet assay and micronucleus scoring with flow cytometry. Mutagenesis. 2018; 33: 77-85.
12. Niidome T, Yamagata M, Okamoto Y, et al. PEG-modified gold nanorods with a stealth character for in vivo applications. Journal of Controlled Release. 2006; 114: 343-347.
13. Alkilany A, Thompson LB, Boulos SP, et al. Gold nanorods: Their potential for photothermal therapeutics and drug delivery, tempered by the complexity of their biological interactions. Advanced Drug Delivery Reviews. 2011; 64: 190-9.
14. Hassan AA, Abdoon ASS, Elsheikh SM, et al. Effect of acute gold nanorods on reproductive function in male albino rats: Histological, morphometric, hormonal, and redox balance parameters. Environ Sci Pollut Res. 2019; 26: 15816-15827.
15. Mehanna ET, Kamel BSA, Abo-Elmatty DM, et al. Effect of gold nanoparticles shape and dose on immunological, hematological, inflammatory, and antioxidants parameters in male rabbit. Veterinary World. 2022; 15: 65-75.

16. Abdoon ASS, Al-Ashkar EA, Kandil OM, et al. Efficacy and toxicity of plasmonic photothermal therapy (PPTT) using gold nanorods (AuNRs) against mammary tumors in dogs and cats. Nanomedicine; Nanotechnology, Biology and Medicine. 2016; 12: 2291-2297.

17. Rashad SES, Haggran A, Aboul-Ela EI, et al. Cytotoxic and genotoxic effects of 50nm Gold Nanorods on mouse splenocytes and human cell lines. Egyptian Journal of Chemistry. 2022; 65: 509-514.

18. Nikoobakht B, El-Sayed MA. Preparation and growth mechanism of gold Nanorods (NRs) using seed-mediated growth method. Chem Mater. 2003; 15: 1957-1962.

19. Virkajarvi N, Paakko P, Soini Y. Apoptotic index and apoptosis influencing proteins bcl-2, mcl-1, bax and caspases 3, 6 and 8 in pancreatic carcinoma. Histopathology. 1998; 33: 432-9.

20. Schlörmann W, Glei M. Comet fluorescence in situ hybridization (Comet-FISH): Detection of DNA damage. Cold Spring Harb. Protoc. 2009; 4: 1-6.

21. You J, Zhou J, Zhou M, et al. Pharmacokinetics, clearance, and biosafety of polyethylene glycol-coated hollow gold nanospheres. Particle and Fibre Toxicology. 2014; 11: 26.

22. Chen YS, Hung YC, Liau I, et al. Assessment of the in vivo toxicity of gold nanoparticles. Nanoscale Res Lett. 2009; 4: 858-864.

23. Bekhti FS, Soulimane MN, Bensalah M, et al. Histological Injury to Rat Brain, Liver, and Kidneys by Gold Nanoparticles is Dose-Dependent. ACS Omega. 2022; 7: 20656-20665.

24. Del Monte U. Swelling of hepatocytes injured by oxidative stress suggests pathological changes related to macromolecular crowding. Med Hypotheses. 2005; 64: 818-825.

25. Schrand AM, Rahman MF, Hussain SM, et al. Metal-based nanoparticles and their toxicity assessment. Nanomed Nanobiotechnol. 2010; 2: 544-568.

26. Baudrimont M, Andrei J, Mornet S, et al. Trophic transfer and effects of gold nanoparticles (AuNPs) in Gammarus fossarum from contaminated periphytic biofilm. Environ. Sci. Pollut. Res. Int. 2018; 25: 1181-1191.

27. Yahyaei B, Nouri M, Bakherad S, et al. Effects of biologically produced gold nanoparticles: Toxicity assessment in different rat organs after intraperitoneal injection. AMB Express. 2019; 9: 38.

28. Weaver JL, Tobin GA, Ingle T, et al. Evaluating the potential of gold, silver, and silica nanoparticles to saturate mononuclear phagocytic system tissues under repeat dosing conditions. Particle and Fibre Toxicology. 2017; 14: 25.

29. Lewinski N, Colvin V, Drezek R. Cytotoxicity of nanoparticles, Small. 2008; 4: 26-49.

30. Orabi SH, Mansour DA, Fathalla SI, et al. Effects of administration of 10 nm or 50 nm gold nanoparticles (AuNPs) on blood profile, liver and kidney functions in male albino rats. Indian Journal of Biochemistry and Biophysics. 2019; 57: 486-493.

31. Fraga S, Brandão A, Soares ME, et al. Short- and long-term distribution and toxicity of gold nanoparticles in the rat after a single-dose intravenous administration. Nanomedicine: Nanotechnology, Biology, and Medicine. 2014; 10: 1757-1766.

32. Zhang XD, Wu HY, Wu D, et al. Toxicologic effects of gold nanoparticles in vivo by different administration routes. Int. J. Nanomed. 2010; 5: 771-781.

33. Lau IP, Chen H, Wang J, et al. In vitro effect of CTAB- and PEG-coated gold nanorods on the induction of eryptosis/erythroptosis in human erythrocytes, Nanotoxicology. 2012; 6: 847-56.

34. Kozics K, Sramkova M, Kopecka K, et al. Pharmacokinetics, biodistribution, and biosafety of PEGylated gold nanoparticles in vivo. Nanomaterials. 2021; 11: 1702.

35. Báez DF, Gallardo-Toledo E, Oyarzún MP, et al. The Influence of size and chemical composition of silver and gold nanoparticles on in vivo toxicity with potential applications to central nervous system diseases. Int. J. Nanomed. 2021; 16: 2187-2201.

36. Rambanapasi C, Zeevaart JR, Buntting H, et al. Bioaccumulation and subchronic toxicity of 14 nm gold nanoparticles in rats. Molecules. 2016; 21: E763.

37. Turkez H, Yousef MI, Geyikoglu F. Propolis prevents aluminum-induced genetic and hepatic damages in rat liver. Food Chem Toxicol. 2010; 48: 2741-2746.

38. Baraaj AH, Aitaie MA, Hamoode HR. Evaluation of histological changes in kidney of male albino rats treated with silver nanoparticles. Systematic Reviews in Pharmacy. 2021; 12.

39. Balfourier A, Kolosnjaj-Tabi J, Luciani N, et al. Gold-based therapy: From past to present. Proc. Natl. Acad. Sci. USA. 2020; 117: 22639-22648.

40. Abdal Dayem A, Hossain MK, Lee, SB, et al. The Role of reactive oxygen species (ROS) in the biological activities of metallic nanoparticles. Int. J. Mol. Sci. 2017; 18: 120.

41. Bin-Jumah MN, Al-Abdan M, Al-Basher G, et al. Molecular mechanism of cytotoxicity, genotoxicity, and anticancer potential of green gold nanoparticles on human liver Normal and cancerous cells. Dose Response. 2020; 18: 1559325820912154.

42. Li C, Wang Y, Zhang H, et al. An investigation on the cytotoxicity and caspase-mediated apoptotic effect of biologically synthesized gold nanoparticles using Cardiospermum halicacabum on AGS gastric carcinoma cells. International Journal of Nanomedicine. 2019; 14: 951-962.

43. Lopez-Chaves C, Soto-Alvaredo J, Montes-Bayon M, et al. Gold nanoparticles: distribution, bioaccumulation and toxicity. In vitro and in vivo studies, Nanomed. Nanotechnol. Biol. Med. 2018; 14: 1-12.

44. Paino IM, Marangoni VS, de Oliveira RCS, et al. Cyto and genotoxicity of gold nanoparticles in human hepatocellular carcinoma and peripheral blood mononuclear cells. Toxicol Lett. 2012; 215: 119-25.

45. Abo-Zeid MAM, Liehr T, Glei M, et al. Detection of cyto- and genotoxicity of rod-shaped gold nanoparticles in human blood lymphocytes using Comet-FISH. Cytologia. 2015; 80: 173-181.

46. Sabella S, Carney RP, Brunetti V, et al. A general mechanism for intracellular toxicity of metal-containing nanoparticles. Nanoscale 2014; 6: 7052.

47. Kowsalya E, Christas KM, Jaquline CRI, et al. Gold nanoparticles induced apoptosis via oxidative stress and mitochondrial dysfunctions in MCF-7 breast cancer cells. Appl Organomet Chem. 2021; 35: e6071.